


## High peak power mini-array quantum cascade lasers operating in pulsed mode

Yuhang Zhang(章宇航), Yupei Wang(王渝沛), Xiaoyue Luo(罗晓玥), Chenhao Qian(钱晨灏), Yang Cheng(程洋), Wu Zhao(赵武), Fangyuan Sun(孙方圆), Jun Wang(王俊), and Zheng-Ming Sun(孙正明)

**Citation:**Chin. Phys. B, 2025, 34 (**1**): 014204. DOI: 10.1088/1674-1056/ad886b
Journal homepage: http://cpb.iphy.ac.cn; http://iopscience.iop.org/cpb

**What follows is a list of articles you may be interested in**

---

## Anti-symmetric sampled grating quantum cascade laser for mode selection

Qiangqiang Guo(郭强强), Jinchuan Zhang(张锦川), Fengmin Cheng(程凤敏), Ning Zhuo(卓宁), Shenqiang Zhai(翟慎强), Junqi Liu(刘俊岐), Lijun Wang(王利军),Shuman Liu(刘舒曼), and Fengqi Liu(刘峰奇)
Chin. Phys. B, 2023, 32 (**3**): 034209. DOI: 10.1088/1674-1056/ac7291

## Broad gain, continuous-wave operation of InP-based quantum cascade laser at $\lambda$~11.8 μm

Huan Wang(王欢), Jin-Chuan Zhang(张锦川), Feng-Min Cheng(程凤敏), Zeng-Hui Gu(顾增辉), Ning Zhuo(卓宁), Shen-Qiang Zhai(翟慎强), Feng-Qi Liu(刘峰奇), Jun-Qi Liu(刘俊岐), Shu-Man Liu(刘舒曼), and Zhan-Guo Wang(王占国)
Chin. Phys. B, 2021, 30 (**12**): 124202. DOI: 10.1088/1674-1056/abf91a

## Tunable characteristic of phase-locked quantum cascade laser arrays

Zeng-Hui Gu(顾增辉), Jin-Chuan Zhang(张锦川), Huan Wang(王欢), Peng-Chang Yang(杨鹏昌), Ning Zhuo(卓宁), Shen-Qiang Zhai(翟慎强), Jun-Qi Liu(刘俊岐), Li-Jun Wang(王利军), Shu-Man Liu(刘舒曼), Feng-Qi Liu(刘峰奇), and Zhan-Guo Wang(王占国)
Chin. Phys. B, 2021, 30 (**10**): 104201. DOI: 10.1088/1674-1056/abec30

## Beam steering characteristics in high-power quantum-cascade lasers emitting at ~4.6 μm

Yong-Qiang Sun(孙永强), Jin-Chuan Zhang(张锦川), Feng-Min Cheng(程凤敏), Chao Ning(宁超), Ning Zhuo(卓宁), Shen-Qiang Zhai(翟慎强), Feng-Qi Liu(刘峰奇), Jun-Qi Liu(刘俊岐), Shu-Man Liu(刘舒曼), and Zhan-Guo Wang(王占国)
Chin. Phys. B, 2021, 30 (**3**): 034211. DOI: 10.1088/1674-1056/abd6fe

## An equivalent circuit model for terahertz quantumcascade lasers: Modeling and experiments

Yao Chen (姚辰), Xu Tian-Hong (徐天鸿), Wan Wen-Jian (万文坚), Zhu Yong-Hao (朱永浩), Cao Jun-Cheng (曹俊诚)
Chin. Phys. B, 2015, 24 (**9**): 094208. DOI: 10.1088/1674-1056/24/9/094208

---

# High peak power mini-array quantum cascade lasers operating in pulsed mode

Yuhang Zhang(章宇航)[1], Yupei Wang(王渝沛)[3], Xiaoyue Luo(罗晓玥)[3], Chenhao Qian(钱晨灏)[4], Yang Cheng(程洋)[5], Wu Zhao(赵武)[5], Fangyuan Sun(孙方圆)[5], Jun Wang(王俊)[3,5,†], and Zheng-Ming Sun(孙正明)[2,‡]

[1] *Southeast University–Monash University Joint Graduate School (Suzhou), Southeast University, Suzhou* 215125, *China*
[2] *School of Materials Science and Engineering, Southeast University, Nanjing* 211189, *China*
[3] *College of Electronics and Information Engineering, Sichuan University, Chengdu* 610065, *China*
[4] *Huaiyin Institute of Technology, Huaian* 223003, *China*
[5] *Suzhou Everbright Photonics Co., Ltd., Suzhou* 215163, *China*

(Received 28 July 2024; revised manuscript received 12 September 2024; accepted manuscript online 18 October 2024)

Broad area quantum cascade lasers (BA QCLs) have significant applications in many areas, but suffer from demanding pulse operating conditions and poor beam quality due to heat accumulation and generation of high order modes. A structure of mini-array is adopted to improve the heat dissipation capacity and beam quality of BA QCLs. The active region is etched to form a multi-emitter and the channels are filled with InP:Fe, which acts as a lateral heat dissipation channel to improve the lateral heat dissipation efficiency. A device with $\lambda \sim 4.8$ μm, a peak output power of 122 W at 1.2% duty cycle with a pulse of 1.5 μs is obtained in room temperature, with far-field single-lobed distribution. This result allows BA QCLs to obtain high peak power at wider pump pulse widths and higher duty cycle conditions, promotes the application of the mid-infrared laser operating in pulsed mode in the field of standoff photoacoustic chemical detection, space optical communication, and so on.

**Keywords:** quantum cascade laser, mini-array, thermal management

**PACS:** 42.55.Px, 42.55.–f, 42.60.Da, 42.70.Nq

**DOI:** 10.1088/1674-1056/ad886b **CSTR:** 32038.14.CPB.ad886b

## 1. Introduction

High power quantum cascade lasers have important applications in infrared countermeasures, gas detection, and other fields.[1] Quantum cascade lasers were first demonstrated by Faist *et al.* in 1994[2] and have developed rapidly in recent years. In 2020, Northwestern University produced a device with output power of 5.6 W in continuous wave mode at room temperature, and the wall plug efficiency reached 22%.[3] Diode lasers operating in pulse mode have attracted a lot of attention; it has applications in a variety of industries, including material processing,[4] lidar,[5] surgery,[6] and more. High peak power can be produced in pulse mode, and the material's exposure to thermal effects can be reduced.[7] Laser bars are typically used to obtain high peak power in the near infrared spectrum. The efficiency exceeds 70% and a peak power production of up to kilowatts has been reached.[8] For QCLs, due to its application requirements, including chemical detection and optical communication, peak power and high beam quality are the focus of research in recent years. To obtain higher peak power, increasing the volume of the active region is a simple method, namely broad area quantum cascade lasers. In 2009, Bai *et al.* produced BA QCLs with a ridge width of 400 μm and a cavity length of 4 mm.[9] At room temperature, the peak power reached 120 W with 200-ns pulse width and 0.2% duty cycle. In 2017, Zhao *et al.* obtained a device with a peak power of 62 W by optimizing the material growth in the active region, its ridge width was 400 μm and cavity length was 4 mm.[10] As the ridge width increases, the waste heat generated during operation increases, and the efficiency of the device decreases. At the same time, the high order mode is difficult to suppress, and the far field will display a double-lobed distribution.[9] In 2015, Heydari and Bai *et al.* used an inclined cavity structure to optimize the beam quality.[11] The device's ridge width was 400 μm and cavity length was 4 mm. The peak power reached 203 W at room temperature, with a pulse width of 200 ns and a duty cycle of 0.02%. It had a single beam with a divergence angle of 3°. However, the process of the inclined cavity method is complicated and difficult to produce. In BA QCLs, due to the significant expansion of the width of the active area, the lateral heat dissipation efficiency decreases. Heat is mainly dissipated from the longitudinal waveguide layer, and the central temperature of the

†Corresponding author. E-mail: wjdz@scu.edu.cn
‡Corresponding author. E-mail: zmsun@seu.edu.cn

© 2025 Chinese Physical Society and IOP Publishing Ltd. All rights, including for text and data mining, AI training, and similar technologies, are reserved.

active area further increases. Heat dissipation efficiency limits further improvements in BA QCLs power, and pulse mode output can usually only be achieved with a narrow pump pulse width and low duty cycle. Multi-emitter laser array is one of the viable solutions to solve the heat dissipation problem.[12,13] Different from conventional semiconductor lasers, QCLs can achieve high peak power in a small ridge width, the multi-emitter arrays can be integrated into one chip, greatly reducing the size of the device. In 2012, Naurois *et al*. produced a laser array with 32 emitters, with a peak output power of 230 mW, and evanescent coupling between beams was achieved.[14] In 2012, Chen *et al*. produced an array with five emitters, with a peak power of 4 W at 500 ns and 10 kHz.[15] In 2015, Kirch *et al*. produced a resonant leakage-wave coupling phase-locked array with a peak power of 5.5 W.[16] The peak power is low since the distance between adjacent transmitting electrodes is relatively close, the heat dissipation is inadequate, and the number of emitters is limited.

In this work, to improve BA QCLs' ability for dissipating heat and beam quality, mini-array quantum cascade laser (MA QCL) was designed. The optimal ridge and channel width were simulated to obtain better heat dissipation performance. Then the experimental verification was conducted. The active region is etched to the depth of the bottom InP waveguide layer to generate a mini-array and InP:Fe is used for secondary epitaxial regrowth. This structure improves lateral heat dissipation efficiency, allowing BA QCLs to obtain high peak power at wider pump pulse widths and higher duty cycle conditions. The beams of different emitters overlap together and form a single-lobed far-field profile. QCLs operate in pulse mode has an extensive application prospect due to its wide range of working conditions and high beam quality.

## 2. Simulation and manufacturing

Figure 1 shows the structure of MA QCLs. The structure is grown on an InP substrate using metal–organic chemical vapor deposition (MOCVD) system technology. The active region is composed by alternate growth of InGaAs/InAlAs with a designed wavelength of 4.8 μm.[17] The growth sequence is: lower layer (InP, Si, $2\times10^{16}$ cm$^{-3}$, 3 μm), forty stages of active region, upper waveguide layer (InP, Si, $1\sim3\times10^{17}$ cm$^{-3}$, 4 μm), contact layer (InP, Si, $1\times10^{19}$ cm$^{-3}$, 0.65 μm). After that, the wafer is etched at equal intervals to form channels with the width of $D$, leads to separated active regions with the width of $d$. Then a secondary epitaxy is performed and the channel is filled with InP:Fe. A 4-μm-thick layer of gold is electroplated on the SiN insulation layer to help dissipate heat. Chips were bonded P-side down on the SiC substrate with AuSn solder.

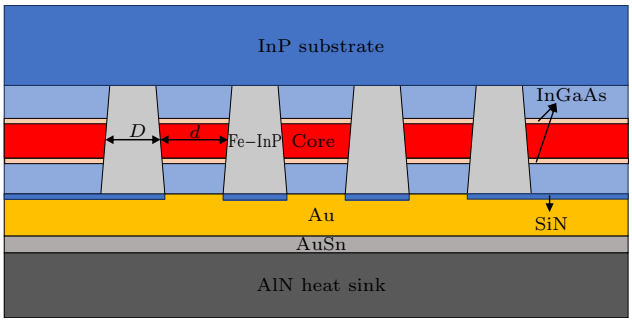



**Fig. 1.** Simplified structure of MA QCLs. Partial ridges are shown in the figure. $D$ is the width of channel, which is filled with InP:Fe. $d$ is the width of ridge.

To study the impact of the mini-array structure on heat dissipation efficiency, finite element method was used to conduct thermal simulations of the device. The bottom of the SiC substrate was set to 288 K, simulating the temperature of platform in actual testing. Since the small size of the device, it is assumed that the thermal convection and thermal radiation can be ignored. Each micro ridge acts as a 1.5-μs, 8-kHz pulse mode output independent heat source with a heat source density of $2.88\times10^{14}$ W/m$^3$. The transient heat transfer equation is given by

$$\rho C_{\mathrm{p}}\frac{\partial T}{\partial t}=\nabla\cdot(k\nabla T)+Q, \tag{1}$$

where $\rho$ is the material density, $C_{\mathrm{p}}$ is the specific heat of the material, $k$ is the thermal conductivity of the material, and $Q$ is the heat source density in the active region. Considering the superlattice structure of the active region, its thermal conductivity is set to be anisotropic, and $k_{\perp}$ is approximately 20% of $k_{\parallel}$.[18] Figure 2 shows the effects of ridge width $d$ and InP:Fe regrowth width on peak temperature. The volume of the active region is the same and the effective width is 300 μm. As figure 2(a) shows, the change in temperature of the active area region when ridge width increases from 3 μm to 10 μm was calculated while $D=8$ μm. As $d$ increases, the peak temperature gradually increases and the growth rate gradually decreases. After $d>8$ μm, the peak temperature changes relatively slowly. As figure 2(b) shows, the change of center temperature in the active region as regrowth width grows from 1 μm to 10 μm was calculated for $d=5$ μm. As regrowth width grows, the peak temperature steadily falls, and the temperature becomes constant when regrowth width approaches 10 μm. This indicates that at this regrowth width, there is minimal thermal interaction between adjacent ridges. Based on the simulation results, MA QCLs' heat dissipation performance improves when the InP:Fe regeneration width increases and the ridge width decreases. Figure 3 shows the heat flux distribution of BA QCLs with a ridge width of 300 μm and MA QCLs with $d=5$ μm and $D=10$ μm. The active region volume of the two constructions is the same. Heat is primarily dissipated from the longitudinal in BA QCLs due to the wider

active region width and high transverse to longitudinal ratio. The transverse heat dissipation efficiency is just 0.12%. For MA QCLs, the filling of InP:Fe permits part of the heat to dissipate from the sides and prevents heat accumulate in active region. The lateral heat dissipation accounts for 45.92%. The peak temperature of MA QCLs with $d = 5$ μm and $D = 10$ μm is 34 K lower than that of BA QCLs under the same conditions. The mini-array structure improves BA QCLs' heat dissipation capacity closer to typical QCLs.[19]

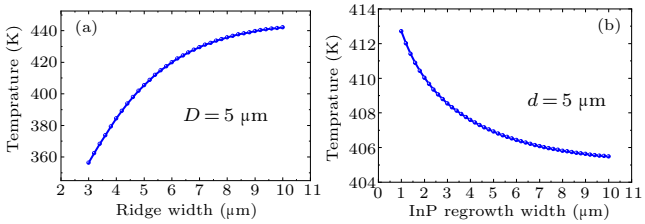



**Fig. 2.** Effects of ridge width $d$ and InP:Fe regrowth width $D$ on the peak temperature of MA QCLs. (a) Effect of ridge width on device peak temperature when $D = 10$ μm, (b) effect of InP:Fe regrowth width on device peak temperature when $d = 5$ μm.

The wafer was processed into a double-channel ridge waveguide laser with an average core width of 300 μm. Devices with three different parameters were fabricated. The channel width $D$ was 10 μm, the ridge width $d$ was 8 μm, 6 μm, and 5 μm, while the effective width of the active region was all 300 μm. BA QCLs with an active area width of 300 μm were produced for comparisons. InP:Fe was then used for re-growth. SiN of 350 nm was deposited on the upper surface. 4-μm Au was deposited for better heat dissipation performance. After cleaving with a 5-mm cavity length, coating was applied on the front and rear cavity facets, while the high-reflectivity (HR) coating consists of $Y_2O_3$/Ti/Au/$Y_2O_3$. Chips were bonded on the SiC substrate with AuSn solder epi-side down. Figure 4 shows the cross-section SEM image of the MA QCLs.

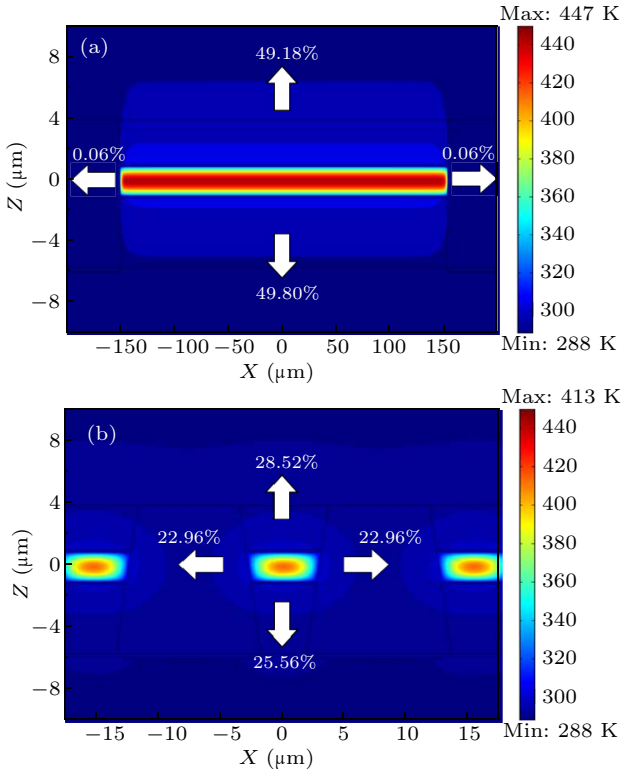



**Fig. 3.** Temperature and heat flux distribution of BA QCLs and MA QCLs.

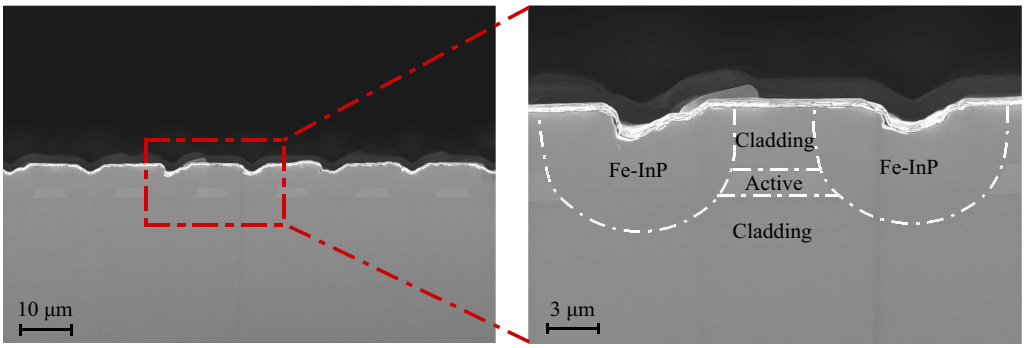



**Fig. 4.** SEM images of the cross-section of the device.

## 3. Results

All tests were conducted under pulsed current conditions with a pulse width of 1.5 μs and a frequency of 8 kHz. The chip was secured using a mechanical clamp, and the bottom of the sink was contact with a temperature-controlled platform maintained at 15 °C. The average power was measured using a thermopile power detector (Gentec), and the actual peak power was calculated from the duty cycle. Spectrum was collected using a Fourier transform infrared spectrometer (FTIR) using a resolution of 1 $cm^{-1}$. Figure 5 shows the *L–I–V* and WPE characteristics of devices with different ridge widths. The device with $d = 5$ μm obtained a peak power of 122 W at 82 A. The threshold current is 22 A, the slope efficiency is 2.92 W/A, the maximum WPE reaches 10.6%, and the threshold current density is 1.47 kA/$cm^2$. As the ridge width decreases, rollover of current occurs later, leading to higher peak power. This is consistent with the conclusion obtained from previous simulations that greater ridge width is associated with worse heat dissipation efficiency at the same InP:Fe regrowth width. How-

ever, as the effective width of the active region is constant, the number of emitters grows while the ridge width decreases. As a result, the waveguide loss of device increases, which raises the threshold current. Results for BA QCLs are also shown in the picture. Due to the influence of heat, the slope efficiency decreases, and the chip is prone to failure with the rear cavity surface damaged. Figure 6 shows the far-field measured at 30 A for MA QCLs with different ridge widths. The far-field divergence angles of ridge widths of 8 μm, 6 μm, and 5 μm are 35.2°, 28.1°, and 26.3°, respectively. Compared with the distinct dual-lobed far-field of BA QCLs, the far-field profile of MA QCLs presents a single-lobed distribution.[12,20,21] The beams overlap to form a single-lobe far field. A decrease in the ridge width leads to an increase in the total active region width, the far-field divergence angle of lateral direction decreases accordingly.

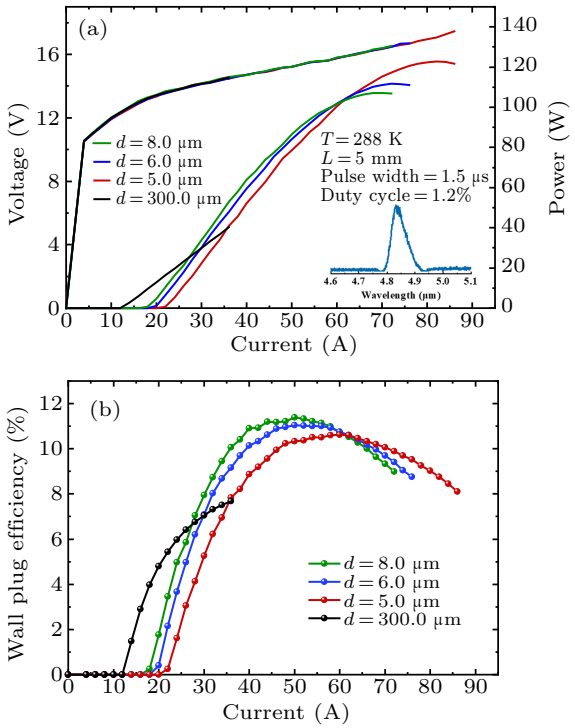



**Fig. 5.** The *L*–*I*–*V* and WPE characteristics of different ridge widths. The cavity length of the device is 5 mm, the effective width of the active region is 300 μm, and $D = 10$ μm.

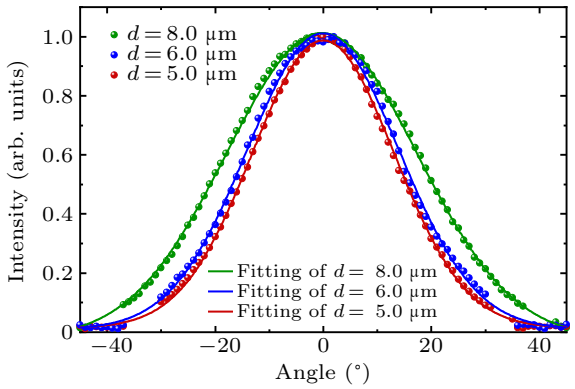



**Fig. 6.** Far-field of lateral direction with different ridge widths.

## 4. Conclusion and perspectives

A mini-array structure is employed to improve the heat dissipation capability of wide-ridge quantum cascade lasers. Through two-dimensional finite element thermal simulation, it is found that the peak temperature of MA QCLs is reduced by 34 K compared with BA QCLs. Based on the simulation results, devices with different ridge widths were fabricated. Under the operating conditions of $T = 288$ K, a pulse width of 1.5 μs, and a frequency of 8 kHz, a device with a ridge width of 5 μm achieved a peak power of 122 W at 82 A, and the maximum WPE reached 10.6%. Its far-field profile presents a Gaussian-like distribution, the divergence angle is 26.3°. This structure allows BA QCLs reach high peak power under wider pump pulse widths and higher duty cycles conditions, and the beam quality is promoted at the same time.

## References


[1] Chen X, Yang C G, Hu M, Shen J K, Niu E C, Xu Z Y, Fan X L, Wei M, Yao L, He Y B, Liu J G and Kan R F 2018 *Chin. Phys. B* **27** 040701

[2] Faist J, Capasso F, Sivco D L, Sirtori C, Hutchinson A L and Cho A Y 1994 *Science* **264** 553

[3] Wang F, Slivken S, Wu D H and Razeghi M 2020 *Opt. Express* **28** 17532

[4] Dutta Majumdar J and Manna I 2011 *International Materials Rreviews* **56** 341

[5] Geiser P, Willer U, Walter D and Schade W 2006 *Appl. Phys.* **83** 175

[6] Plamann K, Aptel F, Arnold C L, Courjaud A, Crotti C, Deloison F, Druon F, Georges P, Hanna M, Legeais J M, Morin F, Mottay É, Nuzzo V, Peyrot D A and Savoldelli M 2010 *J. Opt.* **12** 084002

[7] Weber R, Graf T, Berger P, Onuseit V, Wiedenmann M, Freitag C and Feuer A 2014 *Opt. Express* **22** 11312

[8] Frevert C, Bugge F, Knigge S, Ginolas A, Erbert G and Crump P 2016 *High-Power Diode Laser Technology and Applications XIV*, February 13–18, 2016, San Francisco, USA p. 113

[9] Bai Y, Slivken S, Darvish S R, Haddadi A, Gokden B and Razeghi M 2009 *Appl. Phys. Lett.* **95** 221104

[10] Zhao Y, Yan F, Zhang J, Liu F, Zhuo N, Liu J, Wang L and Wang Z 2017 *J. Semicond.* **38** 074005

[11] Heydari D, Bai Y, Bandyopadhyay N, Slivken S and Razeghi M 2015 *Appl. Phys. Lett.* **106** 091105

[12] De Naurois G M, Carras M, Simozrag B, Patard O, Alexandre F and Marcadet X 2011 *AIP Adv.* **1** 032165

[13] Gu Z H, Zhang J C, Wang H, Yang P C, Zhuo N, Zhai S Q, Liu J Q, Wang L J, Liu S M and Liu F Q 2021 *Chin. Phys. B* **30** 104201

[14] De Naurois G M, Carras M, Simozrag B, Alexandre F and Marcadet X 2012 *Novel In-Plane Semiconductor Lasers XI*, January 21–26, 2012, San Francisco, USA, p. 305

[15] Chen X, Cheng L, Guo D, Li J Y and Choa F S 2012 *CLEO: Science and Innovations*, May 6–11, 2012, San Jose, USA, p. CTh3N.7

[16] Kirch J D, Chang C C, Boyle C, Mawst L J, Lindberg D, Earles T and Botez D 2015 *Appl. Phys. Lett.* **106** 061113

[17] Botez D, Kirch J D, Boyle C, Oresick K M, Sigler C, Kim H, Knipfer B B, Ryu J H, Lindberg D, Earles T, Mawst L J and Flores Y V 2018 *Opt. Mater. Express* **8** 1378

[18] Lee H K, Chung K S, Yu J S and Razeghi M 2009 *Physica Status Solidi (a)* **206** 356

[19] Lee H K and Yu J S 2010 *Solid-state Electronics* **54** 769

[20] Xu Y, Sun Y, Li W, Ma Y, Zhuo N, Liu J, Zhang J C, Zhai S Q, Liu S M, Wang L J and Liu F Q 2022 *Opt. Express* **30** 36783

[21] Gaolei C, Huan Z, Chenren Y, Haiqing Z, Gangyi X and Li H 2020 *Infrared Physics & Technology* **109** 103427